Research article

Robotic automotive paint curing using thermal signature feedback

Fan Zeng, Beshah Ayalew and Mohammed Omar
Mechanical Engineering, Clemson-University-International Center for Automotive-Research, Greenville, South Carolina, USA

Abstract
Purpose – The purpose of this paper is to present a new closed-loop radiative robotic paint curing process that could replace less efficient and bulky convection-based paint curing processes in automotive manufacturing.
Design/methodology/approach – The proposed robotic paint curing processes uses an Ultraviolet LED panel for a heat source, an infra-red camera for non-contact thermal signature feedback of cure level, and a robot control strategy that incorporates the cure-level information in an inverse dynamics control of the robotic manipulator. To demonstrate the advantage of the closed-loop process in improving cure uniformity, detailed models and discussions of the irradiation process, the robotics and the control strategy are presented.
Findings – A simulation-based comparison of the closed-loop robotic curing with the open-loop robotic curing clearly shows the benefits of using thermal signature feedback in improving cure level uniformity.
Originality/value – This is a new approach proposed to exploit immerging technology and improve the efficiency of energy use in an automotive manufacturing process without sacrificing product quality.

Keywords Robotics, Control technology, Paints, Infra-red devices, Sensors

Paper type Research paper

1. Introduction

Paint provides indispensible protection to car bodies in addition to marketable aesthetic functions. As such paint coating and curing processes form a very important part of automotive manufacturing. Generally, current paint curing processes involve the use of traditional convection or bake ovens installed along the manufacturing line (Mills, 2005). However, this oven-based curing method suffers from high energy losses and long working times, both of which reduce the efficiency of the curing process and thereby increase manufacturing costs.

To address these shortcomings of convection-based paint curing, some new radiation-based technologies are being developed, one of which is Ultraviolet (UV) curing. In this approach, UV radiation is applied on temperature sensitive substrates, such as wood, paper and plastic (Schwalm, 2007). Due to its advantages of energy saving, reduction in working time and solvent-free formulation, the UV curing method is becoming more and more attractive.

The early method for applying UV curing processes on automotive bodies is to create a tunnel containing many fixed UV lamps, the positions of which are designed off-line to provide uniform radiation over the entire target surface. This method replaces the traditional oven with an array of UV lamps, which can cure the target surface quickly but require re-design of lamp arrangements for different car body styles or targets. The required uniformity cannot always be achieved because of the complex geometry of some target surfaces. In order to address these issues, a robotic UV curing approach has been proposed (Mills, 2005). The configurations of these two approaches of UV curing are shown in Figure 1. Note that proper UV safety enclosures are necessary for both approaches.

When compared with the fixed UV-lamp array method, the robotic UV curing method requires effective, robust and reliable operation of the UV lamp installed on the end effector of the manipulator. The motion of the robot should also be designed to ensure that it can deliver the appropriate energy to the target surface. Different car bodies may require re-design of the motion of the robot, which can be achieved to some degree through calibration without any hardware modification. To make this robotic curing process more flexible and adaptive as well as to ensure a higher level of cure uniformity, this paper proposes an improved method which can achieve an online adjustment of robot's motion by using curing level feedback via thermal signature information.

The rest of this paper is organized as follows. Section 2 describes the configuration of the proposed robotic curing system. Section 3 outlines trajectory planning and motion control, and this is followed by a discussion of the adopted model for analyzing the curing process in Section 4. Section 5 outlines a simulation of the process and presents the results from this study.

2. Configuration of the System

The basic idea of the proposed closed-loop robotic UV curing method is illustrated in Figure 2. The system consists of the following components:

The current issue and full text archive of this journal is available at **www.emeraldinsight.com/0143-991X.htm**

Industrial Robot: An International Journal
36/4 (2009) 389–395
 [ISSN 0143-991X]
[DOI 10.1108/01439910910957165]

Figure 1 Two types of UV curing for automobile bodies: fixed UV lamp array (left), and robotic UV lamp curing (right)

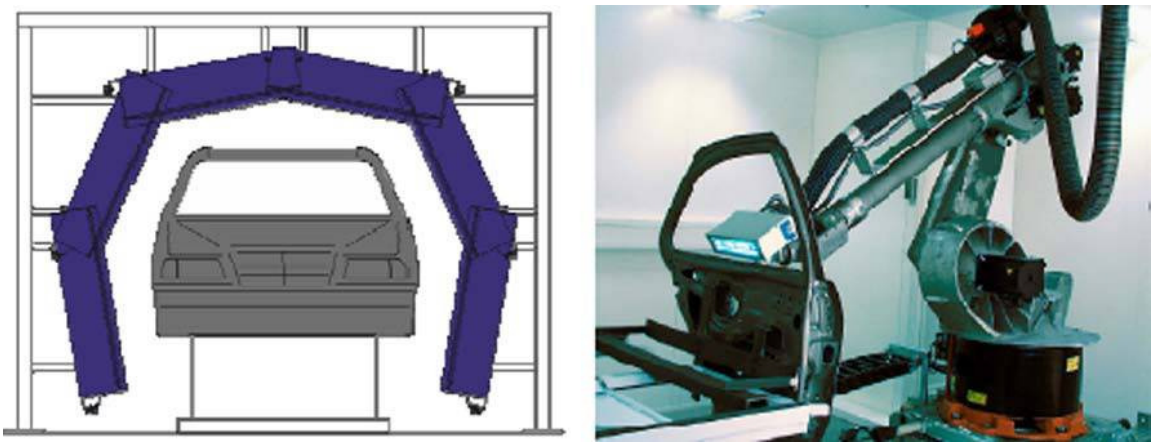

Source: Mills (2005)

Figure 2 Configuration of the robotic UV curing system with thermal signature feedback

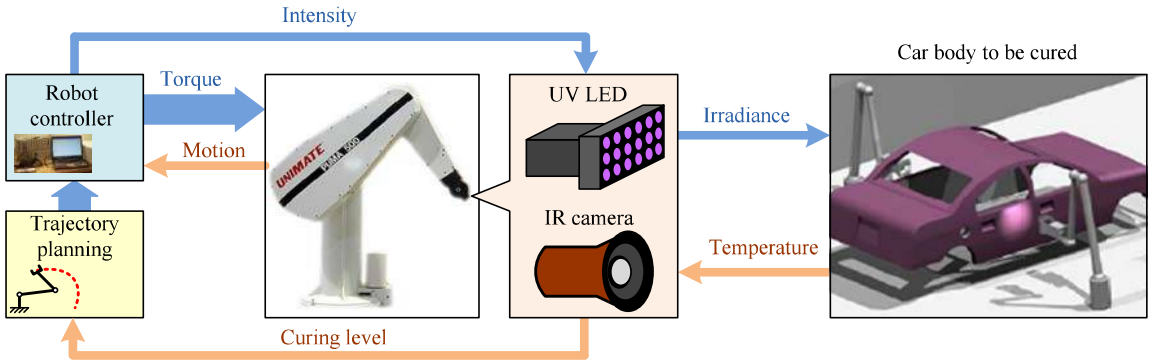

- *Manipulator and controller.* A general 6DOF industrial manipulator, such as PUMA560 adopted for this analysis, can be used to execute the curing process. Since the motion of the robot should be adapted online based on the cure-level feedback information, a suitable controller and adaptive trajectory planning are required to compute the appropriate join torques and ensure that the robot can cure the target surface correctly.
- *UV source.* Instead of traditional UV lamp with reflector, a UV LED array can be included in the curing system due to its extremely long lifetime and nearly instant on/off capacity. The UV LED is installed on the end effector of the manipulator and its intensity can ideally be adjusted by a controller according to the feedback information provided by the IR camera.
- *IR camera.* The IR camera is also installed on the end effector of the manipulator and can be used to monitor the temperature distribution of the target surface, which indicates the corresponding curing level. The information obtained by the IR camera is sent back to the controller to adjust the robot's motion and the intensity of the UV LED so that the desired curing level can be achieved.

3. Trajectory planning and motion control

One of the most important tasks in robotic curing is moving the end effector along some designed path over the target surface so that it can be irradiated by the UV LED appropriately. This task is addressed in two parts.

3.1 Trajectory planning

Generally, the goal of trajectory planning is to generate the reference input for the controller so that the manipulator is directed to execute the desired task successfully (Sciavicco and Siciliano, 2001). Trajecotry planning typically follows in two steps: the first is designing the end effector's path in geometry domain (operational space) and the second is planning the corresponding time history for each joint in time domain (joint space). Typically, path design is performed in operational space of the manipulator in order to describe the task easily, while trajectory planning is done in joint space to generate the time sequences of reference position, velocity and acceleration for the robot controller.

3.1.1 Path design

The basic task of path design is to find an appropriate path for the end effector to cover the whole target surface uniformly and effectively. Usually, a simple way is to move the end effector over the target surface with a constant speed. At the same time, the normal direction of the UV LED will be kept perpendicular against the target surface and the distance between them should also be constant in order to ensure the uniformity. However, this method can only be effective on regular surfaces, such as planes, cylinders, etc. It is much harder to achieve good cure level uniformity by sweeping the

end effector over a complicated target surface, like a car body, with a constant speed.

In this work, a feedback-based discrete method is proposed to generate the desired path taking into account cure level feedback. Figure 3 shows the two different path designs. The sweep method is an open-loop process (Raith, *et. al.*, 2001), while the second method is a closed-loop cure process.

The second method shown in Figure 3 follows a two-step strategy to execute the curing process. First, the end effector will be moved from the current position to the next one quickly. Then it will stay there until the curing process of that area has been done. The time the end effector stays in an area is determined by the feedback information from the IR camera. This strategy makes it possible for the robot to cure a complicated target surface by itself without any human-based and zone specific calibration work. More details about this approach are discussed in the following subsection.

3.1.2 Trajectory planning

When the path design for the manipulator is completed, the desired path of the end effector is generated in the operational space in terms of some key points. This path is a special time law selected to generate the time sequences of the end effector's position and orientation. Then, an inverse kinematics algorithm will be implemented to get the corresponding time sequences of each joint's position, velocity and acceleration in order to extract the desired robot configuration. Generally, the end effector's position and orientation can be represented as the following standard form (Paul, 1982; Zomaya, 1992):

$$T = \left[\begin{array}{ccc|c} & \overset{3\times3}{R} & & \overset{3\times1}{p} \\ \hline 0 & 0 & 0 & 1 \end{array}\right] \quad (1)$$

In the above matrix T, R is a 3×3 sub-matrix which denotes the orientation of the end effector's local coordinate and p is a 3×1 vector representing the position of the origin of this local coordinate. The two terms describe the relationship between the end effector's local coordinate system and the global coordinate system for the manipulator. Since the desired path has been quantized by some key points, the orientation and position of the end effector for each point can also be characterized by a set of matrices for each point in the sequence: $T_1, T_2, T_3, \cdots, T_n$, as shown in Table I.

By using an inverse kinematics algorithm, the orientation and position of the end effector in the operational space can be re-described in the joint space in terms of joint angles. For a 6 DOF manipulator as considered in this work, this step requires calculating six joint angles for each matrix, which represents the orientation and position of the end effector at each point. This can be seen from Table I.

The transformation between the operational space and joint space can be achieved by using a recursive inverse kinematics algorithm as illustrated in Figure 4 (Sciavicco and Siciliano, 2001).

In Figure 4, T_r denotes one of the desired trajectory matrices which describes the position and orientation of the end effector. $\mathcal{J}$ is the Jacobian matrix which describes the differential kinematics of the manipulator. $T(q)$ represents the matrix calculated by the estimated joint angles q and will be compared with the desired matrix T_r to get the position and orientation difference e. The above calculation is repeated for a few times until the difference $e$is approximately zero. In this manner, the joint angles corresponding to the desired matrix T_r is computed. After all desired joint angles have been calculated for each point of the path listed in Table I, a special

Figure 3 wo methods for path design: sweep (top) and curing level feedback (bottom)

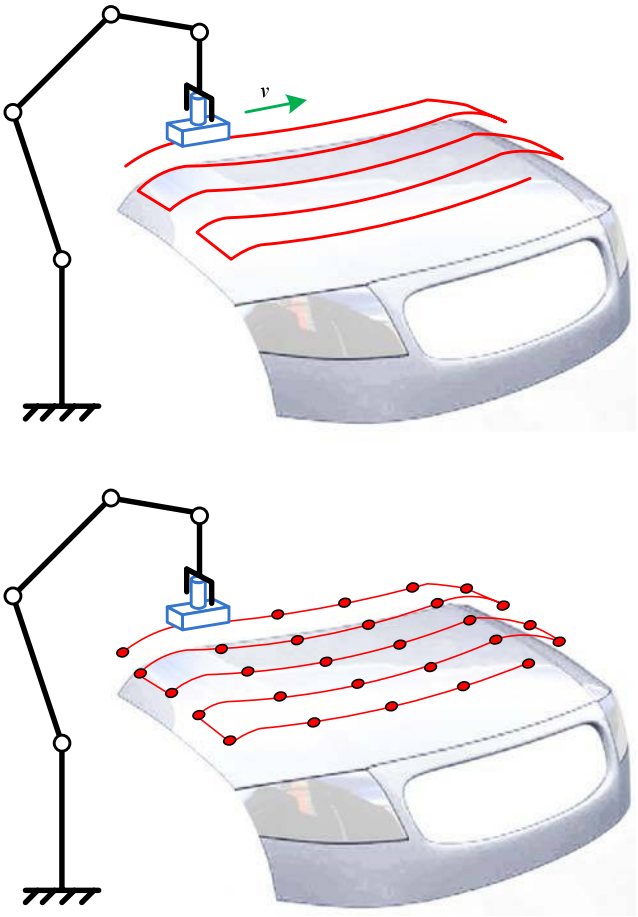

Table I Transformation between operational space and joint space

Operational space	Joint space					
T_1	q_1^1	q_2^1	q_3^1	q_4^1	q_5^1	q_6^1
T_2	q_1^2	q_2^2	q_3^2	q_4^2	q_5^2	q_6^2
T_3	q_1^3	q_2^3	q_3^3	q_4^3	q_5^3	q_6^3
...			...			
T_n	q_1^n	q_2^n	q_3^n	q_4^n	q_5^n	q_6^n

Figure 4 Block diagram of the recursive inverse kinematics algorithm

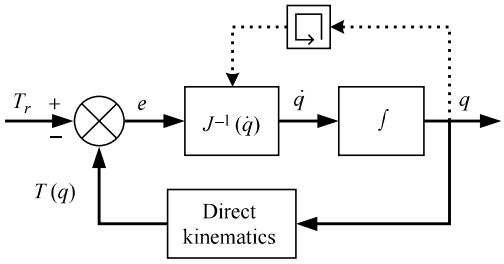

Industrial Robot: An International Journal
Volume 36 · Number 4 · 2009 · 389–395

time law is applied to generate the trajectory of joint angle, velocity and acceleration in time domain. This gives the discrete motion of the end effector.

In Figure 5, q_i, $\dot{q}_i$ and $\ddot{q}_i$ represent the angle, velocity and acceleration of the ith joint, respectively, $(i = 1, 2, \cdots, 6)$. q_i^j and q_i^{j+1} denotes the angles of the ith joint at two adjacent points. t_j and t_{j+1} represent the start-moving time for point j and point $j+1$. $t_{j+1/2}$ denotes the end-moving time for point j. Then the moving time duration between points j and $j+1$, and the stopping time duration at point $j+1$ can be calculated by the following expressions, respectively:

$$\Delta t_{\text{moving}} = t_{j+1/2} - t_j \tag{2}$$

$$\Delta t_{\text{stopped}} = t_{j+1} - t_{j+1/2} \tag{3}$$

In this work, the moving time duration is designed as a constant based on the characteristic time response of the manipulator and UV LED, while the stopping time is determined online by the feedback information of curing level from the IR camera. As is shown in Figure 5, the trajectory during the moving stage is designed as a spline type in order to smooth the joint's motion. Since the inverse kinematics has been done off-line according to Table I and equation (1), the trajectory planning process becomes simple and only requires determining the stopping (hold) time duration at each point based on feedback of curing level information.

3.2 Motion control

In the previous section, the trajectory planning process has generated the reference inputs for the controller of the manipulator. Now the task of motion control is to determine the time history of torques exerted on each joint to ensure that the end effector can follow the desired trajectory. Several control strategies can be implemented to solve this problem, including general PID control, inverse dynamics control and so on. In this work, inverse dynamics control is adopted, as it is effective in eliminating the nonlinearity and coupling of the system from a theoretical point of view. It simplifies the control of the motion of the manipulator to a linear and decoupled second-order problem which can be easily dealt with to achieve a near perfect tracking of the desired trajectory.

Figure 5 Trajectory of joint angle, velocity and acceleration between two adjacent path points

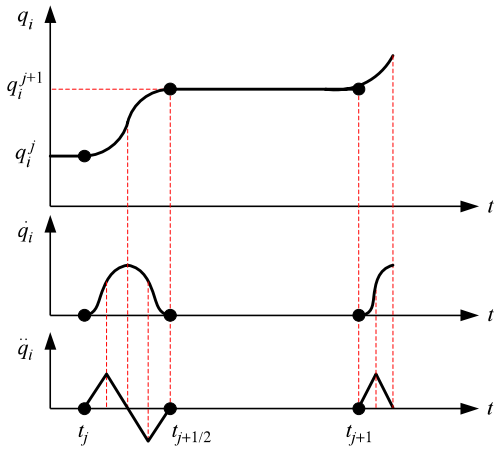

Generally, the dynamics of the 6DOF manipulator can be described by the following differential equations:

$$D(\vec{q})\ddot{\vec{q}} + C(\vec{q}, \dot{\vec{q}})\dot{\vec{q}} + G(\vec{q}) = \vec{\tau} \tag{4}$$

In Equation (4), $\vec{q}$ and $\dot{\vec{q}}$ are vectors describing the positions and velocities of the six joints. The matrix $D(\vec{q})$ contains the effective inertia of each joint and the coupling inertias between joints. $C(\vec{q}, \dot{\vec{q}})$ is the matrix representing the centrifugal and Coriolis effects. $G(\vec{q})$ is a vector describing the gravity load at each joint. All of these items are determined by both physical parameters and current state of the manipulator (Paul, 1982; Sciavicco and Siciliano, 2001; Pires, 2006).

According to the feedback linearization method, the controller can be designed as follows to eliminate those nonlinear items in Equation (4):

$$\vec{\tau} = C(\vec{q}, \dot{\vec{q}})\dot{\vec{q}} + G(\vec{q}) + D(\vec{q})\vec{v} \tag{5}$$

$$\vec{v} = -K_V\dot{\vec{q}} - K_P\vec{q} + (\ddot{\vec{q}}_d + K_V\dot{\vec{q}}_d + K_P\vec{q}_d) \tag{6}$$

Here,$\vec{q}_d$, $\dot{\vec{q}}_d$ and $\ddot{\vec{q}}_d$ denote the reference inputs generated by the trajectory planning process. $\vec{q}$ and $\dot{\vec{q}}$ are the actual position and velocity of the joints. $D(\vec{q})$,$C(\vec{q}, \dot{\vec{q}})$ and $G(\vec{q})$ can be obtained by inverse dynamics calculation. K_v and K_p are coefficient matrices which can be chosen to enforce a desired tracking error dynamics (Slotine and Li, 1991).

4. Modeling the irradiation process

The UV curing process is critically influenced by the exposure of the target to UV radiation and the corresponding thermo-chemical response of the paint components. In this paper, we assume that the chemical parameters have been pre-specified for this automotive application, and the distribution of the cure level on the target surface is predominantly determined by the exposure process.

To model the exposure process, two important aspects should be considered: the UV radiator and the target receiver. In this work, we select a portable UV LED array as the radiator, which consists of a number of UV cells. Each cell can be considered as an ideal Lambertian point source as depicted in Figure 6 (Ashdown, 1994).

Figure 6 illustrates the distribution of the radiant intensity of the lambertian point source at the vertical section of an emissive sphere. The corresponding radiant intensity (W/sr) of an arbitrary point on this sphere can be characterized as a function of the angle between the emissive direction and the normal direction of the source:

Figure 6 The lambertian point source

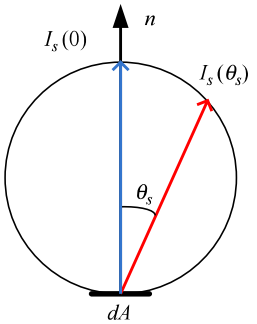

$$I_s(\theta_s) = I_s(0) \cdot \cos\theta_s = \frac{\phi}{\pi} \cdot \cos\theta_s \tag{7}$$

Here, $I_s(0)$ denotes the radiant intensity at the normal direction of the source and ϕ is the radiant flux (W) which is also one of the most significant parameters of a UV cell. Obviously, the radiant intensity at other directions will decrease with the increasing of the emissive angle θ_s. Due to the complexity of the target surface which is not always a simple sphere, the power density arriving at the receiver is not only determined by the radiator but also greatly influenced by the geometric configuration between the radiator and receiver (Siegel and Howell, 1981; Modest, 1993).

Figure 7 shows a general radiative exchange between an emissive element and a receiving element. In Figure 7, n_s and n_r represent the normal directions of the emissive and receiving elements, respectively. θ_s and θ_r are emissive and receiving angles. dA_s and dA_r denote the areas of the two elements, and b is the distance between them.

If the emissive element can be simplified as a Lambertian point source, then the irradiance (W/m^2) arriving at the receiving element can be characterized by:

$$E_r = \frac{[\phi/\pi \cdot \cos\theta_s] \cdot (dA_r \cdot \cos\theta_r)/b^2}{dA_r} = \frac{\phi \cdot \cos\theta_s \cdot \cos\theta_r}{\pi b^2} \tag{8}$$

It can be seen from the above expression that the irradiance at the receiving element is greatly influenced by the geometric configuration between the radiator and receiver. Smaller distances between the radiator and receiver will lead to an increasing irradiance at the target surface, which may improve the speed of the curing process. That is one of the most important reasons why we try to use a manipulator to execute the curing process. Since, the UV LED array is constituted by a lot of Lambertian-type cells, the irradiance arriving at one patch of the target surface can be obtained by using the superposition principle as shown in Figure 8.

Different patches of the car body have different properties due to the unevenness during the welding, forming and painting processes. Accordingly, the irradiance arriving at the car body cannot be absorbed at a uniform extent. This effect can be modeled by adding a location dependent efficiency factor to the irradiance expression:

$$E_r = k \cdot \frac{\phi \cdot \cos\theta_s \cdot \cos\theta_r}{\pi b^2} \tag{9}$$

Figure 7 Radiative exchange between an emissive and a receiving element

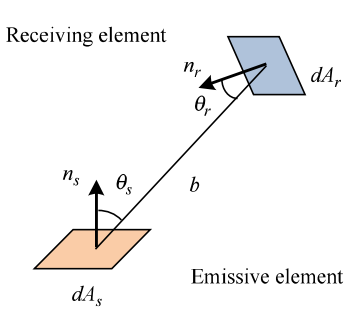

Figure 8 Radiation superposition from all UV cells at a patch of the car body

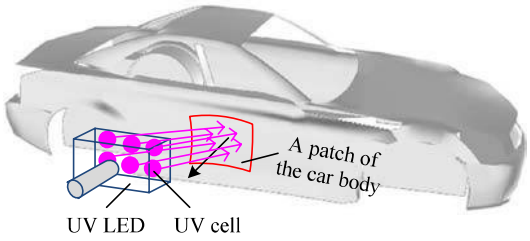

The factor k is used in this work only to model nonuniformity effects for demonstrating the closed loop curing process using simulations, as will be discussed in the next section.

Now we can calculate the total power absorbed by one patch of the car body by:

$$P(x,y,z,t) = \int_{As}\int_{Ar} k \cdot \frac{\phi \cdot \cos\theta_s \cdot \cos\theta_r}{\pi b^2}\, dA_r dA_s \tag{10}$$

Then the corresponding energy absorbed by the same patch can be obtained by integration of the power:

$$E(x,y,z,t) = \int_0^t P(x,y,z,t)\mathrm{d}t \tag{11}$$

Both the power and energy expressions are functions of coordinate and time, because the irradiance and the associated efficiency factor are determined by the geometric configuration between the UV LED and the car body. This geometric configuration is also time-variant due to the movement of the UV LED installed on the end effector. Therefore, the curing level, which can be mapped into the absorbed energy and associated temperature proportionally, is also a function of both coordinate and time. In this work, the curing level is considered to be detected by an IR camera, which captures the thermal signature of the patch covered by the camera. At each time step, the average temperature of that patch indicates the current curing level of the same patch, and can be sent back to the controller to determine the appropraite motion command for the manipulator to cure the next patch.

5. Simulation results

In this section, we will simulate the above robotic UV curing process in MATLAB/Simulink and the multi-body dynamics software SIMPACK. The latter is used to establish the dynamic model of a PUMA 560 manipulator. The controller of the manipulator is implemented in MATLAB/Simulink based on the inverse dynamics control algorithm outlined in Section 3. The irradiation proccess, the UV LED and IR camera are also modeled in MATLAB/Simulink. Since the controller, the process and the manipulator are developed in different environments, co-simulation between MATLAB/Simulink and SIMPACK is executed to achieve a simulation of the curing process. Figure 9 shows the manipulator and a simple cure target as modeled in SIMPACK.

Figure 10 shows the block diagram of the total system. The trajectory planning block generates the reference joint position (q0), velocity (dq0) and acceleration (ddq0) for the controller in real-time based on the default path design and the feedback curing level information. According to the

Figure 9 The manipulator model and the cure target modeled in SIMPACK

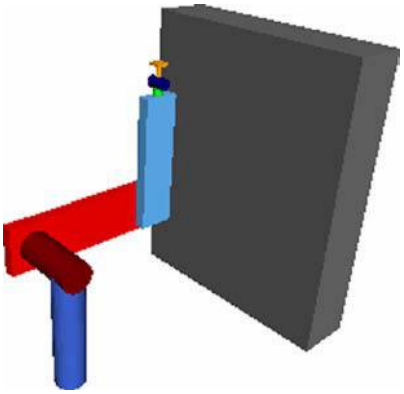

inverse dynamics strategy, the controller calculates the joint actuator torque based on the reference inputs and the actual joint position (q) and velocity (dq) from SIMPACK. Then the torque will be sent to the manipulator model established in SIMPACK where the actual joint position and velocity are calculated and exported. The direct kinematics block will transform the joint position into the end effector's position and orientation accordingly. Finally, the curing process block estimates the curing level of the current patch based on the end effector's position and orientation, the radiation model and the IR camera model.

Figure 11 shows the details of the curing process model for an example configuration that is used to demonstrate the proposed process in this work. The target surface (1.4 × 0.3 m) is quantized into a 140 × 30 grid. Similarly, the UV LED and IR camera are quantized into two 10 × 10 grids and the distance between them is 0.03 m. Here, it is assumed that the UV LED is at the center of the end effector and the IR camera can directly measure the energy distribution of the patch covered by the UV LED. Therefore, this distance also denotes the one between the end effector and the target surface. To model the unevenness of the target surface, we simply assign 65 × 30 cells on the far left with a low efficiency factor of 0.8 and the right 65 × 30 cells on the far right with a high factor of 1. Those 10 × 30 cells in the middle have a gradual-changed factor between 0.8 and 1. The end effector will follow a round-trip linear path which is also shown in Figure 11. Two trajectory strategies, including the open-loop sweep method and the discrete but closed-loop move-stop-move one will be implemented and compared. For the curing level feedback method (closed-loop), fourteen stop points are assigned at the first half path and thirteen stop points are assigned at the second half with a 5-cell shift from the last stop point of the first half path. Figure 12 shows MATLAB simulation results for the target surface cured using the two methods.

The color maps in Figure 12 represent the curing level distribution of the whole 140 × 30 grid, which is varying from 0.2 to 1 according to the color band shown. Figure 13 shows the corresponding curing level distribution along the designed path based on the calculation of the average of the energy distribution.

It can be seen from Figures 12 and 13 that, the constant-speed sweep method cannot compensate for the unevenness of the radiative characteristics of the target surface due to the open-loop nature of this method. However, it can be seen that the curing level feedback method achieves better cure level uniformity since it considers both the desired and actual curing level information in determining the motion of the end effector.

6. Conclusions

In this paper, a closed-loop robotic curing process has been proposed and simulated. The system consists of a UV-LED for a heat source, and an IR-camera for thermal signature feedback, and a robotic manipulator. An inverse dynamics controller is derived and a strategey is devised to use the cure-level information obtained from the thermal camera.

A multi-domain simulation of the robotic curing process is conducted to demonstrate the function. An open-loop robotic curing process (called the sweep method) is compared with a closed-loop robotic curing process proposed in this work. The results show that the closed loop process maintains better uniformity in the face of non-uniform absorption efficiencies by the target surface.

Further, work is being pursued to experimentally verify the benefits of closed- loop curing as simulated in this work and consider variations in curing system layout and test other control schemes. The authors own several IR cameras that can image objects with high spatial and temperature resolutions (minimum resolvable temperature difference

Figure 10 The block diagram of the total system

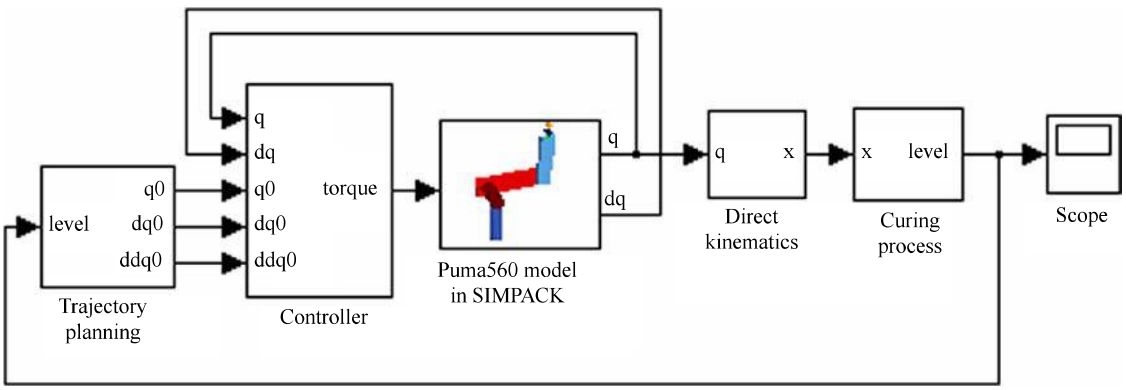

Figure 11 The model of the curing process

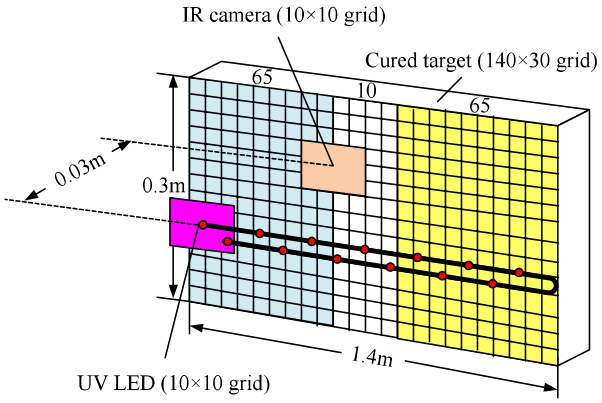

Figure 12 Energy distribution of the target surface under the two methods

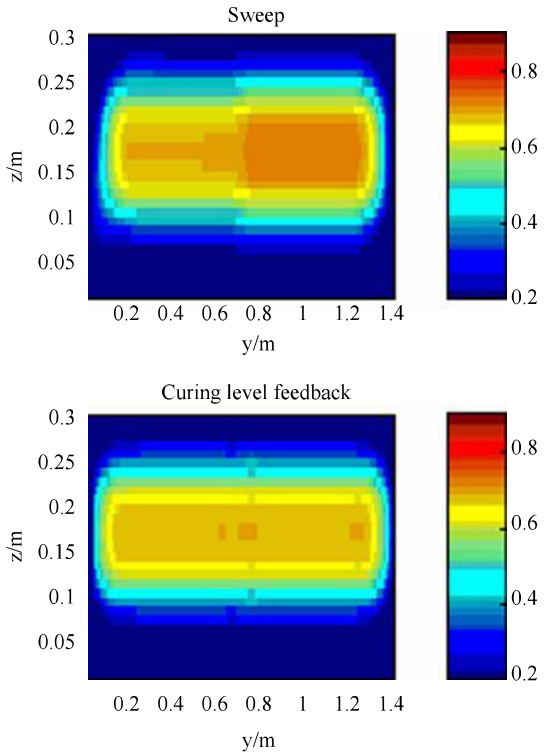

MRTD of 0.1 mK and 640 × 512 pixel), with focus at less than 10 cm (from the target). The proposed system can work well with an industrially packaged micro-bolometric camera or a cooled indium-antimonite InSb array. A commercially availble example is the ThermaCAM® SC6000 (Infrared Systems, 2008). In addition, UV LED panels are also already available commercially (Dymax Corp, 2008). Such available solutions have led the authors to believe that the proposed

Figure 13 The average energy distribution along the path

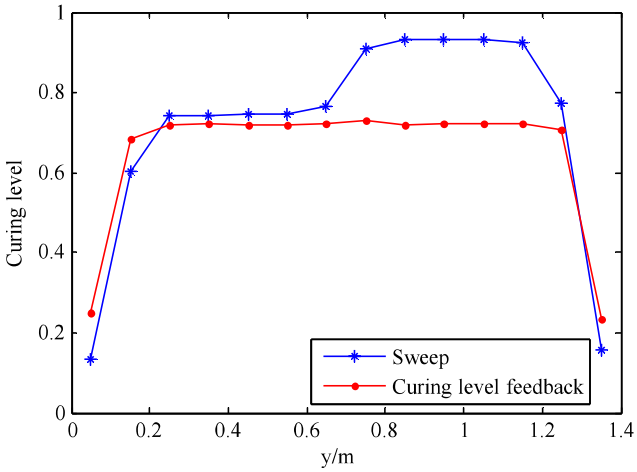

closed-loop curing systems are technologically quite feasible today.

References

Ashdown, I. (1994), *Radiosity: A Programmer's Perspective*, Wiley, New York, NY.

Dymax Corp (2008), "Curing systems", available at: www.dymax.com/

Infrared Systems (2008), "Infrared cameras", available at: www.infraredsys.com/index.html

Mills, P. (2005), "Robotic UV curing for automotive exterior applications: a cost-effective and technically viable alternative for UV curing", North American Automotive UV Consortium Report, Strongsville, OH.

Modest, M.F. (1993), *Radiative Heat Transfer*, McGraw Hill, New York, NY.

Paul, R.P. (1982), *Robot Manipulators: Mathematics, Programming, and Control*, MIT Press, Cambridge, MA.

Pires, J.N. (2006), *Industrial Robots Programming: Building Applications for the Factories of the Future*, Springer, New York, NY.

Raith, T., Bischof, M.M. and Gemmler, E. (2001), "3-D UV technology for OEM coatings", RadTech Report Article on Robotic UV Curing at Daimler Chrysler, Germany.

Schwalm, R. (2007), *UV Coatings: Basics, Recent Developments and New Applications*, Elsevier, Amesterdam.

Sciavicco, L. and Siciliano, B. (2001), *Modeling and Control of Robot Manipulators*, Springer, London.

Siegel, R. and Howell, J.R. (1981), *Thermal Radiation Heat Transfer*, Hemisphere Publishing Corporation, Washington, DC.

Slotine, J.J. and Li, W. (1991), *Applied Nonlinear Control*, Prentice Hall, Englewood Cliffs, NJ.

Zomaya, A.Y. (1992), *Modeling and Simulation of Robot Manipulators: A Parallel Processing Approach*, World Scientific, Singapore.

Corresponding author

Fan Zeng can be contacted at: fzeng@clemson.edu